Journal of Cleaner Production 462 (2024) 142648

Contents lists available at ScienceDirect

Journal of Cleaner Production

journal homepage: www.elsevier.com/locate/jclepro

An integrated model with interdependent water storage for optimal resource management in Energy–Water–Food Nexus

Muhammad Babar Rasheed [a,b,*], María D. R-Moreno [a]

[a] Universidad de Alcalá, Escuela Politécnica Superior, ISG, Alcalá de Henares, Spain
[b] University of Gloucestershire, Cheltenham, GL53 0QA, UK

ARTICLE INFO

Handling Editor: Kathleen Aviso

Keywords:
Power flow
Water flow
Water storage
Food network
Locational marginal pricing

ABSTRACT

With the rapid increase in population and the industrial revolution, the demand for clean energy and water has substantially increased, underscoring their importance for sustainable economic development. Although energy and water infrastructures are often viewed as separate and uncoupled due to distinct processes in power generation and water production, they are fundamentally interlinked within their respective domains. This necessitates a strong coupling to optimally manage power and water resources simultaneously. To address this, a joint optimization algorithm has been developed to manage the supply-side resources of the Energy–Water–Food Nexus (EWFN), including the power, water, food, cogeneration, and storage networks. A mathematical model is first developed to dispatch clear power, potable water, and storage resources, considering constraints related to supply, demand, production, flow, and ramping. Additionally, the integration of a water storage facility alleviates binding constraints, enabling flat production to reduce costs and CO_2 emissions. The proposed methodology also allows for the real-time quantification of production costs, energy mix, reserve and curtailed capacities, and energy imbalances. This methodological extension to EWFN includes flexible resources within the grid's portfolio to promote cleaner production, ensuring that the required amount of water is consumed across all sectors. Finally, the proposed algorithm is tested on freely available datasets, demonstrating that the co-dispatch of energy and water resources in the presence of constraints leads to optimal generation and distribution of power and water without heavily relying on a single-product plant.

1. Introduction

The relentless surge in the global population, advancements in the industrial sector, and the pressing concerns of climate change have significantly magnified the challenges in optimally utilizing power and water resources to cater to escalating demands (Rogers, 2013; Averyt et al., 2013). The quest for sustainable development in both residential and commercial sectors increasingly hinges on the availability of green, carbon-neutral energy sources and access to potable water (Kanyerere et al., 2018). In recent times, there has been a heightened focus on the interconnected infrastructure of energy, water, and food networks, a concept encapsulated in the Energy–Water–Food Nexus (EWFN) (Probst et al., 2024). Traditionally, the systems that deliver power and water, catering to diverse sectors including residential, commercial, food processing, and agriculture (Al-Ansari et al., 2017), have been viewed as distinct entities. Yet, the reality presents a more integrated scenario where these infrastructures are inherently coupled (Peña-Torres et al., 2024), functioning synergistically (Farid and Lubega, 2013; Lubega and Farid, 2014).

Recognizing the intertwined nature of these systems (as detailed in Table 1), it becomes evident that the energy and water infrastructures necessitate a unified approach to optimization. This is essential to efficiently supply both energy and water resources, not only to residential and commercial zones but also to the agricultural sector, which is crucial for food production. Accordingly, this study introduces a comprehensive joint optimization program that addresses the combined supply dynamics of power, water, and food. This program includes aspects of power generation, water supply, cogeneration, and water storage facilities (Li et al., 2018). This initiative builds on foundational concepts, integrating generation, flow, demand, ramping, and storage considerations. It extends them to embrace the challenges and opportunities presented by the energy–water–food nexus (Ngammuangtueng et al., 2023).

The overall objective is to manage the available sources (thermal, hydel, solar, renewable, water storage, etc.) without requiring excessive investments in the existing infrastructure (Li et al., 2018). This involves predicting both power generation and consumption behavior

* Corresponding author at: Universidad de Alcalá, Escuela Politécnica Superior, ISG, Alcalá de Henares, Spain.
E-mail address: muhammad.rasheed@uah.es (M.B. Rasheed).

https://doi.org/10.1016/j.jclepro.2024.142648
Received 25 April 2022; Received in revised form 15 May 2024; Accepted 21 May 2024
Available online 25 May 2024

Nomenclature

Number Sets

i	power plant index
j	water plant index
k	cogeneration plant index
t	total no. of hours (t = 24)
n_{pp}	total no. of power plants
n_{cp}	total no. of cogeneration plants
n_{wp}	total no. of water plants
t	total no. of hours (t = 24)

Parameters

μ	variable representing congestion
ρ	density of fluid
σ_v	water level of water storage plant
G	gravity
H	height of water storage plant
$v_{\mathbf{a}}$	Water volume in tank
m_w	Total number of water pipes
$H_{\mathcal{W}_s}$	Pressure head at water outlet
σ_v	Water balance constraint
ω_{ab}	Speed of water pump
$\mathcal{W}_s$	Water storage facility
$\mathcal{V}_{\mathcal{W}_s}$	Volume of water in tank
$\eta_{t,u}$	Energy conservation efficiency
C_p	Cost of supplied energy
$\mathcal{G}_{ab}$	Head gain at nodes
x_{ckp}	power from coproduction plant
$A_{ab}, B_{ab}, C_{a,b}$	Water pump parameters
x_{ckw}	water from coproduction plant
L_{ab}	Water pipe head loss
F_{ab}	Water flow in pipes
d_{ab}	Diameter of water pipe
ℓ_{ab}	Length of water pipe
H_j	Head at node j
S_{ab}	Darcy friction factor
δ	Power angle
$E_{t,u}$	Energy consumption of water pump
$B_{i,j}$	bus susceptance matrix
$\mathcal{P}$	Set of water pipes
R_{tu}	resistance coefficient of water pipes
Q	water flow capacity
P_h	hydraulic power of pump
X_{σ_v}	water released by water storage plant
I_{wjt}	incidence matrix-water network
I_{cky}	incidence matrix-cogeneration network
I_{piy}	incidence matrix-power network

Limits

$\underline{GenPP}$	min. limit of power plants
$\overline{GenPP}$	max. limit of power plants
$\underline{GenWP}$	min. capacity limit of water plants
$\overline{GenWP}$	max. limit of water plants
$\underline{GenCPP}$	min. power limit of cogeneration plants
$\overline{GenCPP}$	max. power limit of cogeneration plants
$\underline{GenCPW}$	min. water limit of cogeneration plants
$\overline{GenCPW}$	max. water limit of cogeneration plants
$\underline{PFlow}$	min. power flow limit
$\overline{PFlow}$	max. power flow limit
$\underline{WFlow}$	min. water flow limit
$\overline{WFlow}$	max. water flow limit
$\underline{WStore_{\sigma_v}}$	min. limit on water storage plant
$\overline{WStore_{\sigma_v}}$	max. limit on water storage plant
$\overline{RRP_i}$	ramp-up ratio of power plant
$\overline{RRP_j}$	ramp-up ratio of water plant
$\underline{r_k}$	lower limit on coproduction ratio
$\overline{r_k}$	upper limit on coproduction ratio
$\overline{RRCP_k}$	ramp-up ratio of coproduction plant
$\overline{RRCW_k}$	ramp-up ratio of coproduction plant
$\underline{\omega_{ab}}$	Min. speed of water pump
$\overline{\omega_{ab}}$	Max. speed of water pump
$\overline{v_{\mathbf{a}}}$	Max. water volume
$\underline{\mathcal{V}_{\mathcal{W}_s}}$	Max. water storage limit

Other Symbols

$C_{pi}(x_{pi})$	cost function of power plants
$C_{wj}(x_{wj})$	cost function of water generation plants
$C_{ck}(x_{ckp,ckw})$	cost function of cogeneration plants
C_G	total cost of object function
x_{ck}	cost function of cogeneration plants
L	Lagrangian of optimal flow problem
P_D	power demand
D_w	water demand
n	water flow exponent
F_{tu}	flow of power from node $i-j$
$Pg_{i,max}$	maximum power generation
$Pg_{i,min}$	minimum power generation
Q_{tu}	flow of water from node $t-u$
H_t	tth nodal head
x_{pi}	cost function of power generation plants
m_w	total no. of pipes
t_d	temperature difference
P_{g_i}	power generation from i plants
δ_i	phase angle at bus i

and reduction in CO_2 emission using advanced optimization & control (Rasheed and R-Moreno, 2021), and data analytics techniques. Secondly, a joint optimization model for co-dispatch of water and power (Santhosh et al., 2013) is developed subject to production, demand, transmission, process, ramping, and storage constraints. Furthermore, the inclusion of power, water and storage facilities helped to alleviate the binding constraints to obtain the balanced generation of power and water with minimum cost (Farid and Lubega, 2013). Furthermore, the joint optimization algorithm is designed to achieve the optimal results systematically. It can serve as a base model to set the control points upon which the single-product plants can also achieve optimal control. In addition, the proposed work explicitly considers and includes water storage which may serve as an intermediate mode of storage for residential & industrial heating, power generation, and/or electric vehicle charging. For this purpose, the standard IEEE 30 bus network (Shahidehpour et al., 2015) and the UK-based Hanoi water network (Ghobadian and Mohammadi, 2023) are considered. This was challenging due to the limits on altering the existing infrastructure system beyond the degree of freedom. This task is efficiently done through combining energy and water generation (i.e., cogeneration) facilities

Table 1
Supply and demand sides coupling of EWFN.

	Power supply	Power demand
Water supply	cogeneration – Thermal desalination – Hydroelectric	– Pumped water – Water distribution – Wastewater recycling
Water demand	Thermal power generation facilities	Residential, industrial and commercial use of water heating & cooling of water
	Food industry – Processing	– Wastewater recycling – Heating & cooling, storing

due to their dependence. Finally, the three tasks mentioned above are integrated to finalize the design, architecture, and implementation of EWFN-based optimal resource management for a sustainable future.

The proposed EWFN nexus system model represents a groundbreaking approach with far-reaching impacts on industry, government, residents, academia, and research organizations, as well as the Gulf Cooperation Council (GCC) countries (Al-Adwani et al., 2023). This model provides a benchmark for industries to manage resources through green production facilities, energy mix, and sustainable food production techniques. It enables a cyclical use of resources, where water from power generation and power from water production are efficiently utilized, alongside storage facilities for both. This system also supports sustainable food production by optimizing agricultural practices and reducing waste. Government bodies and research institutes are encouraged to use this model to develop both short-term and long-term policies for better utilization of existing infrastructures, with necessary modifications. This is crucial as the world rapidly shifts towards green and clean generation (Tao et al., 2020), transmission, storage, and use of energy (Teng et al., 2019), water, and food resources. For instance, the European hydrogen pipeline infrastructure, a vast project linking countries for a common cause, and the GCC's plans to balance supply and demand through an energy mix by 2050, exemplify such initiatives (Zaiter et al., 2023).

This strategy, heavily reliant on integrating distributed and alternative energy resources, including storage facilities and hydrogen (Schröder et al., 2021), also extends to sustainable food production and distribution methods. The energy mix under this new strategy will include clean coal, natural gas, nuclear energy, water facilities, solar and wind power, biofuels, and storage facilities, complemented by sustainable agricultural practices. Moreover, the transition from traditional generation facilities to renewables, considering the health and environmental benefits, could yield significant annual savings, ranging from 1–3.7 billion USD by 2030 (Mueller, 2023). This transition also positively impacts the residential sector through the provision of affordable, green energy, and promotes sustainable food consumption patterns.

This proposed work extends our previous research (Schoonenberg and Farid, 2022), which presented a joint optimization program for the supply side of Energy–Water–Food Nexus (EWFN) couplings, as delineated in Refs. Rasheed and R-Moreno (2021) and illustrated in Fig. 1. The initial part is focused on the modeling of Direct Current Optimal Power Flow (DCOPF) and Optimal Water Flow (OWF), which is further developed in this study. Previously, line limits, power generation, water production limits, and capacity constraints were considered. In this extension, it is observed that including process constraints, line limits, ramping limits, water storage facilities, continuity relationships, water pipes models, water junction model, and water pump model significantly improves the performance of the nexus system while reducing overall costs. Additionally, this paper integrates food processing units into the IEEE 30 bus system at nodes 5&29 (Fig. 2), allowing for a more holistic scheduling of the optimal utilization of power, water, storage, and food processing facilities. This integration addresses the high-cost implications of relying only on single-product plants. Moreover, this study has also incorporated Locational Marginal Pricing (LMP) to reflect changes in total costs needed to meet the additional demand requirements of the next unit. The final optimization algorithm has been implemented on datasets from Hanoi, UK (Ghobadian and Mohammadi, 2023), and the modified IEEE 30-bus network (Shahidehpour et al., 2015), with specific attention to the water requirements of the food industry as obtained from Ellis et al. (2009). The inclusion of food processing units offers a comprehensive view of the EWFN dynamics, enabling a more efficient and sustainable management of resources across the energy, water, and food sectors.

The rest of the paper is organized as follows. Section 2 presents a thorough review of the relevant literature on the Energy–Water–Food Nexus (EWFN), laying the groundwork for the study. Section 3 details the system model developed for this research. In Section 4 previous components are integrated into a unified optimization framework. The simulation setup and the results of applying our joint optimization model are elaborated in Section 5, demonstrating the model's effectiveness in reducing CO_2 emissions and operational costs. Section 6 concludes and proposes directions for future research.

2. Relevant literature on nexus

This section elucidates the foundational literature surrounding the joint optimization of multiple plants within the realms of power, water, and other essential sectors. The concept of jointly optimizing power generation and water production facilities has seen significant evolution over the decades, transitioning from focusing on singular plant optimization to embracing the complexities of multi-plant operations (Tao et al., 2020). Traditionally, models have primarily addressed the optimization challenges of individual plants without integrating a unified problem formulation (Li et al., 2018). However, recent investigations have shifted towards the strategic planning and modeling of hybrid-energy systems encompassing standalone setups, yet with less emphasis on their operational and control aspects (Trifkovic et al., 2013). In an innovative approach undertaken by Lambton College in Sarnia, ON, Canada, a dual-layered optimization and control algorithm has been developed. This method strategically manages distributed energy resources, including wind, solar PV, and hydrogen storage, by considering dynamic load demands as a crucial system input.

To address the integrated challenges posed by coupled problems, Schoonenberg and Farid (2022) have proposed a hetero-functional graph-theoretic approach engineering model with minimum cost flow optimization. This model, rooted in Petri-net-based representations, undergoes a transformation into a canonical quadratic form to simplify computational demands, showcasing its applicability in managing the complex integrations within the hydrogen-natural gas European network. Similarly, Xiao et al. (2017) introduced a framework designed for local energy markets, facilitating the trade between hydrogen and energy. This setup includes a diverse range of stakeholders from load to hydrogen vehicles and storage units, employing an iterative decentralized method to optimize the trading process, thereby mitigating peak load demands.

Expanding upon these foundational works, Mingfei Ben (Ban et al., 2017) and Teng et al. (2019) discuss the architectural framework within an electricity, heat, and hydrogen-based multi-energy storage system using distributed energy resources and a hydrogen storage system. This work is dedicated to significantly enhancing grid flexibility through electricity, heat, hydrogen energy conversion, and storage systems. The combined optimization problem was formulated and solved

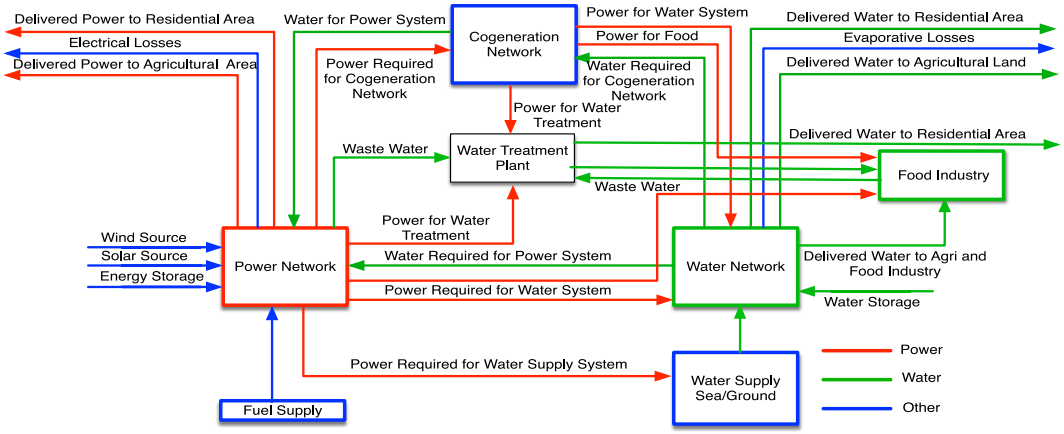

Fig. 1. Topology of the symmetric food–energy–water nexus.

by using an optimal collaborative control theory with the objective of cost reduction. Guangsheng Pan et al. (2020), proposed an electricity-hydrogen integrated energy system planning model with hydrogen production and storage technologies. This model explicitly considers power to heat and hydrogen and seasonal hydrogen storage models with all associated constraints. The objective is to handle the integration challenges through the combination of stochastic & robust optimization techniques. Similar work is proposed to share the resources in a coupled energy system with power-to-gas and plug-in hybrid electric and hydrogen vehicles (PH2EVs) aggregators. Sun and Harrison (2021), develop a supply chain planning model for H2 that determines the least-cost mix of generation, transmission, compression, and storage, facilities to meet H2 demand coupled with the power system. Furthermore, the authors incorporate the flexible scheduling of trucks and pipelines to carry the H2 to serve for transmission and/or storage resources to manage the H2 production/supply/demand across space and time. The work by Sun and Harrison (2021) is dedicated to managing the load demand of hydrogen vehicles in a coupled energy system with the consideration of renewable energy resources. This is because the distributed renewable energy resources pose a serious challenge to the electricity network in the form of intermittent uncertainty, which is handled through on-site hydrogen production and storage.

An economic dispatch model for the day-ahead market of an integrated port energy system considering hydrogen is proposed by Wang et al. (2021), since, the ports are the major source of energy consumption and CO_2 emission. This model includes electricity, natural gas, heat, hydrogen, and renewable energy resources. Hydrogen produced through the water electrolysis is used to power the thermal plants; while the surplus hydrogen capacity can be stored, used, and converted into natural gas through a methanation reaction. Although, this is a great coupled model that manages the dispatch problem in a day-ahead fashion; however, it is difficult to manage all the resources efficiently with less complexity. The work reported by Haggi et al. (2021) has proposed a multi-objective risk-based optimization model to schedule the hydrogen production from water electrolysis, storage, fuel cell, and fueling of hydrogen vehicles. This framework includes integrated demand response, reactive power support from hydrogen systems, and photovoltaic-based renewable energy to provide cheap and interruption-free energy for the electrolysis process. Lin et al. (2021) present another work regarding transmission expansion planning to promote the hydrogen electrolysis process. Water electrolysis is an energy-intensive task that can be performed by either a carbon-based conventional energy source or a carbon-free renewable energy source. In this context, that work identifies that the nonlinear water electrolysis process can be formulated as a feasible region that consists of two subregions. A convex optimization problem is formulated that is solved using mixed-integer nonlinear and later linear programming through relaxing the master problem. Supply chain planning of hydrogen production, transmission, storing, and compression to meet the demand is studied by He et al. (2021). Hydrogen supply through trucks and pipelines is modeled allowing them to manage or shift the hydrogen demand and production across space and time. Later, this hydrogen network is coupled with the electricity network through demand response (DR) pricing programs. Another similar work reported by Tao et al. (2020) is dedicated to solving the energy sharing problem in a coupled electricity and hydrogen network with the objective of social welfare maximization. This study reveals that, unlike energy storage unit integration that has a high cost, power-to-gas and plug-in-hybrid and hydrogen-vehicle aggregators are new coupling points. Zarei (2020) presents a comprehensive survey on a holistic approach to address the security challenges in EWFN. The proposed three-fold schemes jointly optimize the EWFN by integrating multi-objective reservoirs and irrigation ponds to fulfill water demand. This work focused on modeling and optimizing the water sources to meet short and long-term requirements. However, this work does not focus on the optimal production and utilization of power. Another work proposed by Norouzi (2022) presents a systematic approach to analyze the interconnection issues in EWFN.

From the discussion above, it is observed that clean energy and potable water are basic resources that are always required to fulfill current and future needs in such a way as to promote sustainability. However, this is only possible if electric power is generated with reduced CO_2 emissions and supplies potable water with reduced waste. Previously, these demands are fulfilled through independent water and power networks. In contrast, these are now considered as an interlinked network of networks where single and/or multi-products are obtained from within the single facility. On the other hand, with recent developments in renewable energy and hydrogen technologies, the nexus approach is gaining popularity as carbon-free energy can be produced without heavily relying on fossil fuel-based resources and thus can be used in water networks. Although, there has been extensive work done by different authors in energy–water and energy–water–food nexus domains; however, to the author's knowledge, there is no explicit work dealing with the joint optimization framework of power, water, and food networks with water storage facility. In addition, the existing literature does not explore the generation, demand, process, storage, and congestion constraints, simultaneously. Thus, a technique/mechanism that can treat all the plants with equity is required. Then, this technique could be used as a benchmark for the optimization of power and heat plants. Table 2 summarized some relevant research works based on their approaches and methodology to achieve the required objectives. It is also clear from the discussion that numerous works are being developed for EWFN in managing the demand and/or supply-side resources, however, the supply-side coupling with the modeling and integration

Table 2
A comparison of the literature within the nexus framework.

Ref.	Nexus	Technique	Objective	Limitation/Research Gap	Supply-side coupling	Demand-side coupling
Al-Ansari et al. (2017)	EWFN	Life cycle assessment (LCA)methodology	• Integration of greenhouse gas control • waste to power technologies • Evaluate the environmental impact of... • a hypothetical food product system • Biomass integrated gasification • combined cycle • Carbon capture sub-system • Global warming is reduce 80%	EWFN coupling for food processing and delivery system is only evaluated	✗	✓
Zaiter et al. (2023)	EWFN	• A holistic approach • NLP	Power generation cost minimization	Water network modeling, storage integration, ramping limits, continuity relationship are not considered	✓	✗
Zarei (2020)	EWFN	Tinn-Shuan approach is used	Water security challenges	This work theoretically addressed the security challenges	✗	✗
Uen et al. (2018)	EWFN	• A holistic three-fold scheme • Multi-objective optimization • Non-dominated sorting II	• Max. hydropower output • Max. reservoir storage • Simulate long-term water shortage rate	Power generation, optimization and utilization needs more attention	✓	✗
Norouzi (2022)	EWFN	Dynamic system model	Analysis of factor affecting EWFN	Theoretical framework	✗	✗
Santhosh et al. (2013)	EWN	• A holistic approach • NLP	Generation cost minimization	Ramping limits, storage facility, water networks modeling are not considered	✓	✗
Santhosh Apoorva and Youcef-Toumi (2014)	EWN	• A holistic approach • NLP	Power generation cost minimization	Line limits and water networks modeling are not considered	✓	✗
Proposed	EWFN	• A holistic approach • NLP • Joint-optimization	• Power generation cost minimization • Supply–demand balance • Global optimality • Optimal resource utilization	Food network modeling, demand variations, real-time demand profiles, dynamic factors, wastewater treatment, and carbon capture modeling are still missing	✓	✗

of water with storage networks are yet to be explored further. In this context, the proposed work has significant importance and impact on supply-side resource management.

3. System model

This section discusses the proposed system model (Fig. 2) to develop optimization-based control strategies to manage the supply side resources with the objective of cost and CO_2 reductions. Fig. 1 describes the topology of the food–energy–water nexus that includes four power generation plants, three cogeneration plants, one water production plant, and two water storage facilities, respectively. The proposed system model is adopted from our previous work (Rasheed and R-Moreno, 2021) and modified to include the water storage facilities, line & ramping limits, water system models, coupling strategies, and power & water flow constraints. In the considered IEEE 30 bus system, four power plants are located at nodes 2, 3, 8, 13, and three cogeneration plants are placed at nodes 2, 6, 10. The water supply reservoir from the Hanoi water distribution network (Fig. 3) is placed at node 1, where it also provides the water to the power system node 11. The water storage units are located at nodes 14, & 21, respectively. The food processing units are located at nodes 5 and 29. In this way, the power, water, and cogeneration plants are integrated as cyber–physical and nexus systems (Coulbeck, 1980; Salomons, 2010) to meet the demand in various sectors. Consequently, the water network delivers water to the power, cogeneration, and food networks. Similarly, the power network supplies power to the water, cogeneration and water networks. Furthermore, the cogeneration plants provide both the power and water, simultaneously and are generally cheaper than single product power and water plants. Before delving into details, it is pertinent to outline the interrelation of these components within our system model. The foundation is built on optimizing the flows of power and water, addressing the efficiency and sustainability of these critical resources. Direct Current Optimal Power Flow (DCOPF) and Optimal Water Flow (OWF) models form the core, setting the stage for the detailed exploration of infrastructure and operational components crucial for Nexus's functionality. This includes models for water junctions, pipes, and especially water storage facilities, which play a pivotal role in ensuring

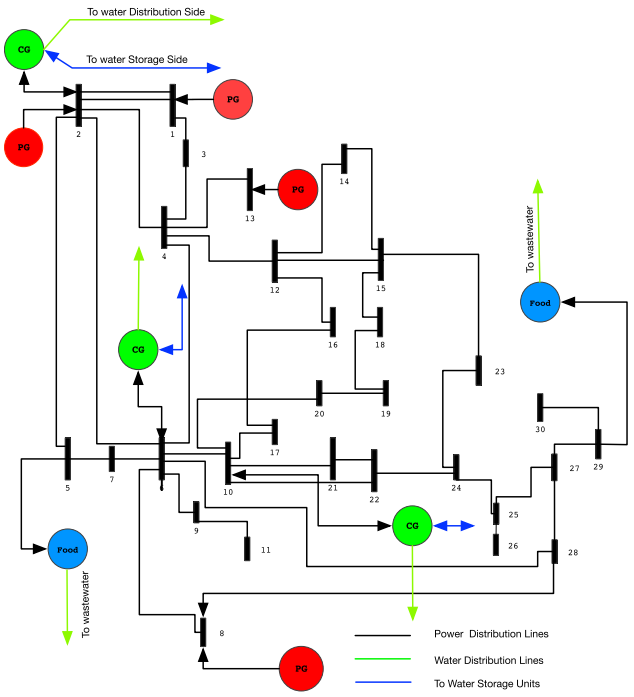

Fig. 2. The modified IEEE standard 30 bus system topology including the power and cogeneration plants. The modified 30-bus system includes the cogeneration facilities at nodes 2, 6, 10.

the resilience and adaptability of the water supply system. Additionally, the energy consumption and associated costs of water distribution are scrutinized, highlighting the economic dimensions of the Nexus. Economic and environmental considerations are woven throughout the model, with locational marginal pricing bringing into focus the balance between cost-efficiency and environmental impact.

3.1. Direct current optimal power flow (DCOPF)

Optimal Power Flow (OPF) methods have advanced to overcome inherent limitations associated with line loading and power flows in traditional Economic Dispatch (ED) models. Therefore, it is essential to integrate transmission and distribution constraints into optimization models. Incorporating limits on power transmission networks not only enhances power system stability but also contributes to the reduction of generation and transmission losses (Leeton et al., 2010). The simplified and deterministic nature of DCOPF models is particularly valued for their analytical and computational benefits (Stott et al., 2009).

This study employs a widely used DCOPF problem formulation based on the system topology, aiming to minimize the total cost of power generation while meeting operational constraints. The formulation incorporates the following components:

- Objective Function: minimizes the total cost of power generation across all periods and plants.

$$min \quad C_{pi}(x_{pi}) = \sum_{t=1}^{T} \sum_{i=1}^{n_{pp}} \left\{ C_{pi,t}(x_{pi,t}) \right\} \tag{1}$$

  Here, $C_{pi,t}(x_{pi,t})$ represents the cost function for power generation at plant i at time t, with $x_{pi,t}$ indicating the generation amount.
- Power Balance Constraint: ensures the balance between power generation and demand at each time interval, adherence to generation capacity limits, and power flow limits.

$$P_{gi,t} - P_{Di,t} = \sum_{y=1}^{m_p} \left\{ B_{yz}(\delta_y - \delta_z) \right\}, \forall t \in T, \tag{2}$$

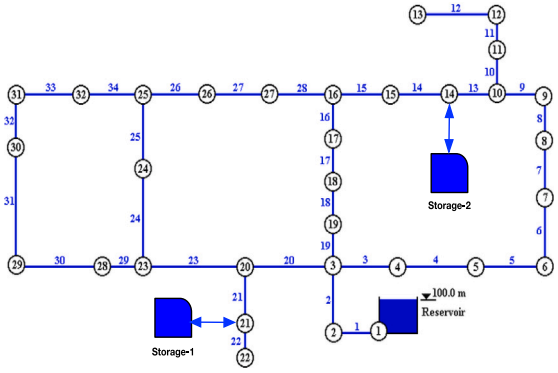

Fig. 3. The modified layout of the water distribution network obtained from Hanoi, UK (Ghobadian and Mohammadi, 2023). In the modified layout, two water storage facilities are integrated at nodes 14 & 21.

where $P_{gi,t}$ and $P_{Di,t}$ denote the generation and demand, respectively, and B_{yz} is the bus incidence matrix.

- Generation Capacity Constraints: maintains generation within min and max limits.

$$\underline{P_{gi,t}} \le P_{gi,t} \le \overline{P_{gi,t}}, \forall t \in T, \tag{3}$$

- Power Flow Limits: constraints on power flow through transmission lines to prevent overloading.

$$\underline{p_{yz,t}} \le p_{yz,t}(B_{yz}(\delta_y - \delta_z)) \le \overline{p_{yz,t}}, \ \forall \ t \in T, \tag{4}$$

- Reference Bus and Voltage Magnitude: standardizes phase angle measurements and voltage levels across the network. It constrained that the power angle at the reference bus is zero and the voltages at power network nodes are fixed at 1 per unit in the DCOPF setting.

$$angle(\delta = 0), \ \& \ |V_i| = 1(p.u), \tag{5}$$

In the DCOPF model, the indices represent different entities within the energy system, denoted by i, j, and k indexes, corresponding to power plants, water facilities, and cogeneration facilities, respectively. The cost functions associated with operating power plants ($C_{pi}(x_{pi})$), water facilities ($C_{wj}(x_{wj})$), and cogeneration facilities ($C_{ck}(x_{ckp,ckw})$) are integral to the objective function.

Given this context, the objective function of Eq (1) has been extended to also consider the costs associated with water production and cogeneration processes:

$$\begin{aligned} min \quad & C_{total}(x_{pi}, x_{wj}, x_{ckp,ckw}) \\ & = \sum_{t=1}^{T} \left(\sum_{i=1}^{n_{pp}} C_{pi,t}(x_{pi,t}) + \sum_{j=1}^{n_{wp}} C_{wj,t}(x_{wj,t}) + \sum_{k=1}^{n_{cp}} C_{ck,t}(x_{ckp,t}, x_{ckw,t}) \right) \end{aligned} \tag{6}$$

This expanded objective function aims to minimize the total cost of operation, considering not only the generation of power but also the production of water and the operation of cogeneration facilities that simultaneously produce power and water. The indices n_{pp}, n_{wp}, and n_{cp} denote the number of power plants, water facilities, and cogeneration plants, respectively. This comprehensive approach ensures that the optimization considers the intertwined nature of energy and water resources, reflecting the complex dynamics of modern integrated energy systems.

3.2. Optimal water flow

This study's water distribution system includes a network of pipes, pumps, supply reservoirs, junctions, pressure valves, and storage tanks. To streamline the model, pumps and valves are categorized as specific

types of pipes, each with a single point for water flow control. This system is represented as a directed graph $\mathcal{G} = (\mathcal{N}, \mathcal{L})$, where $\mathcal{N}$ denotes the nodes – including tanks, reservoirs, and junctions – and $\mathcal{L}$ represents the directed pipes connecting these nodes, indicated as (ab, ba).

3.3. Model of water junctions

The water network comprises junctions (j), with j belonging to the set J where $(|j| = J)$. Dynamic water demand at these junctions, D_{wt} (measured in m^3/s), varies over the time interval t and is applied accordingly for each $j \in J$. It also assumed the D^t_{wt} is known for $j \in J$ over $t \in T$. The notation ab refers to a pipe facilitating the flow Q_{ab} from node a to b, with each pipe ensuring unidirectional water flow within the network. The model prioritizes maintaining flow continuity and balancing supply with demand, alongside managing pressure losses throughout the network. This equilibrium at any junction $j \in J$ is expressed as:

$$D^t_{wa} = \sum_{a=1}^{n_w} \left(\sum_{a \in f_{in}(b)} Q^t_{ab} + \sum_{c \in f_{out}(b)} Q^t_{b,c} \right), \ \forall\ j = 1, \ldots, m_w, \tag{7}$$

where nodes $a \in f_{in}(b)$ supply water to, and $c \in f_{out}(b)$ transport water from, junction b. The overall water flow balance, crucial for network stability, is determined by:

$$F_{ab} = \sum_{a=1}^{n_w} \{Q_{ab} + D_{wa}\}, \ \forall\ j \in m_w, \tag{8}$$

indicating F_{ab} as the net flow, with m_w as the total number of water pipes. Pressure loss across pipes, an essential factor for system operation, follows the relationship:

$$H_a - H_b = R_{ab} Q_a |Q_b|^{n-1}, \tag{9}$$

with the operator maintaining pressure at each junction to satisfy minimum head requirements. Let H^t_b denotes the current pressure head to satisfy the required minimum head level $\underline{H^t_b}$ at time t :

$$H^t_b \geq \underline{H^t_b}, \tag{10}$$

Further, water flow calculation is simplified as:

$$Q_{ab} = \frac{H_a - H_b}{R^{0.54}_{ab} |H_a - H_b|^{0.46}}. \tag{11}$$

The minimum pressure head to ensure adequate water flow is:

$$H_{j,t} \geq \underline{H_j}, \ \forall\ j \in m_w, \& \ t \in T, \tag{12}$$

with the chosen value of n critically influencing pressure head loss calculations. The Hazen–Williams and Darcy–Weisbach formulas, with $n = 1.852$, are commonly used for this purpose (Haktanır and Ardıçlıoğlu, 2004).

3.4. Model of water pipes

The calculation of head loss in water pipes (ab) at each time interval t employs the Darcy–Weisbach equation:

$$L^t_{ab} = f_{ab} \times (Q^t_{ab})^2 \tag{13}$$

Here, f_{ab} represents a non-negative friction factor, defined as $f_{ab} = \frac{f_{ab} \ell_{ab}}{2 d_{ab} S^2_{ab} g} \geq 0$, where ℓ_{ab} and d_{ab} are the length and diameter of the pipe (in meters), respectively, g stands for the acceleration due to gravity (in m/s^2), and S_{ab} indicates the pipe's cross-sectional area. This equation quantifies the energy loss due to friction as water flows through a pipe.

Pressure at each node must adhere to specific limits, ensuring safe operational conditions:

$$0 \leq \underline{H_j} \leq \overline{H_j} \tag{14}$$

where $\underline{H_j}$ and $\overline{H_j}$ denote the minimum and maximum pressure head at node j during time t. These constraints apply universally across junctions J, with $\underline{\mathbf{H}} = \underline{H_j} | j \in J$ representing the array of minimum head pressures, and $\mathbf{D} = \overline{D_{wt}} | j \in J$ encompassing the water demands.

Water storage dynamics are modeled through the balance of tank volumes over time:

$$v^t_a = v^{t-1}_a + F^t_{ab} \tag{15}$$

$$0 \leq v^t_a \leq \overline{v^t_a} \tag{16}$$

Eq. (16) establishes the permissible volume range within a tank, with $\overline{v^t_a}$ specifying the maximum capacity at time t. This framework ensures the continuity and adequacy of water supply while accounting for the physical laws governing fluid motion and system constraints.

3.5. Energy consumption & Cost of pump

Pumps are categorized within the pipeline network, identified by the set $\mathcal{P}$ where each pipe, denoted by $(ab \in \mathcal{P})$, can function as a pump. These pumps facilitate head gain at node (ab) over time t, represented as $\mathcal{G}^t_{ab}$. Considering variable-speed pumps enhances the model's flexibility, allowing for precise control over water supply. The head gain due to pump operation is calculated by:

$$\mathcal{G}^t_{ab} = A_{ab} (Q^t_{ab})^2 + B_{ab} Q^t_{ab} \omega^t_{ab} + C_{ab} (\omega^t_{ab})^2 \tag{17}$$

Here, ω^t_{ab}, $\underline{\omega^t_{ab}}$, and $\overline{\omega^t_{ab}}$ represent the actual, minimum, and maximum speeds of the pump, with A_{ab}, B_{ab}, and C_{ab} being the pump-specific parameters evaluated at nominal conditions.

$$\underline{\omega^t_{ab}} \leq \omega^t_{ab} \leq \overline{\omega^t_{ab}}, \forall t \in T \tag{18}$$

Eq. (18) shows the upper and lower limits of the pump, while the net power to drive a hydraulic pump requires (i) mass flow rate, (ii) liquid density, and (iii) differential height. Let $E^t_{t,u}$ denotes the energy consumption of a hydraulic pump over time t, which is calculated as (Eq. (19)):

$$E^t_{ab} = \frac{1}{\eta_{ab}} \left(\rho \times g \times h \times \mathcal{G}^t_{ab} \times \sum_{a=1}^{n_w} Q^t_{ab} + D_{wa} \right) \tag{19}$$

where ρ is the fluid density (kg/m^3), g is the acceleration due to gravity (m/s^2), h is the vertical lift or height (m), and η_{ab} denotes the pump's energy efficiency, assumed constant over time t. The total energy cost for pumping, C^t_p, integrating real-time energy pricing β^t, is given by:

$$C^t_p = \beta^t \left[\frac{1}{\eta_{ab}} \left(\rho \times g \times h \times \mathcal{G}^t_{ab} \times \sum_{a=1}^{n_w} Q^t_{ab} + D_{wa} \right) \right] \tag{20}$$

This equation calculates the pumping system's operational cost, factoring in the dynamic pricing from electricity markets, thereby enabling an efficient allocation of resources based on real-time cost assessments.

3.6. Water storage model

This work integrates the water storage facility $\mathcal{W}_s$ as a node within the network. The volume of water within $\mathcal{W}_s$ at time t, denoted by $\mathcal{V}^t_{\mathcal{W}_s}$, plays a crucial role in maintaining the system's water balance. The dynamics of water storage, including inflow and outflow, contribute to the balance and are subject to constraints ensuring the volume remains within operational bounds. Eq. (21) describes the water volume's temporal progression, factoring in the net flow – the difference between inflow and outflow – over period t. The subsequent Eq. (22) ensures the volume at any given time adheres to predefined limits, to safeguard against overflow or depletion.

$$\mathcal{V}^t_{\mathcal{W}_s} = \mathcal{V}^{t-1}_{\mathcal{W}_s} + \left(\sum_{a \in f_{in}(b)} Q^t_{ab} - \sum_{c \in f_{out}(b)} Q^t_{b,c} \right) \tag{21}$$

$$\underline{\mathcal{V}^t_{\mathcal{W}_s}} \le \mathcal{V}^t_{\mathcal{W}_s} \le \overline{\mathcal{V}^t_{\mathcal{W}_s}} \tag{22}$$

Additionally, the model accounts for the pressure head at $\mathcal{W}_s$, which fluctuates in response to changing storage volumes and demand. This relationship is encapsulated by:

$$H^t_{\mathcal{W}_s} - H^{t-1}_{\mathcal{W}_s} = \left(\sum_{a \in f_{in}(b)} Q^t_{ab} - \sum_{c \in f_{out}(b)} Q^t_{b,c} \right) \tag{23}$$

Here, Eq. (23) illustrates how the pressure head adjusts with net water flow, highlighting the storage facility's adaptive capacity to meet demand or accommodate surplus supply.

4. Problem formulation

This section synthesizes the problem formulation that integrates the diverse components, explained in the previous section, into a unified framework for optimization, marked by specific operational constraints that ensure system balance and resource optimization. It is developed considering three network types as discussed in Section 2. The objective function is designed to manage network flows within the nexus domain, incorporating water storage facilities, line limits, constraints, and LMP. The primary goal of the primal problem formulation is to minimize the operational costs associated with power and water plants.

$$\begin{aligned} min \quad & \sum_{t=1}^{T} C_{G,t}(x_{pi}, x_{wj}, x_{ck}) \\ & = \sum_{t=1}^{T} \left\{ \sum_{i=1}^{n_{pp}} C_{pi,t}(x_{pi}) + \sum_{j=1}^{n_{wp}} C_{wj,t}(x_{wj}) + \sum_{k=1}^{n_{ck}} C_{ck,t}(x_{ckp,ckw}) + \sum_{s=1}^{n_s} C_{\mathcal{W}_s} \right\} \end{aligned} \tag{24}$$

where, $C_{pi}(x_{pi})$ denotes the cost functions of the ith power generation plant, $C_{wj}(x_{wj})$ is the cost coefficients of jth water production plant, and , $C_{ck}(x_{ckp,ckw})$ is the cost functions of kth cogeneration plant, respectively. In this work, the quadratic cost functions are used in their respective decision variables as given (Eq. (25)):

$$\begin{aligned} & C_{pi,t}(x_{pi}) = a_{2i} x^2_{pi} + a_{1i} x_{pi} + a_{0i} w_{pi,t} \\ & C_{wj,t}(x_{wj}) = \left(a_{2k} x^2_{wj} + a_{1j} x_{wj} + a_{0j} w_{cwj,t} \right) - c_{\mathcal{W}_{s,t}} \\ & C_{ck,t}(x_{ckp,ckw}) = a_{11k} x^2_{ckp} + a_{22k} x^2_{ckw} + \left(a_{12k} x_{ckp} x_{ckw} - c_{\mathcal{W}_{s,t}} \right) \\ & \quad + a_{1k} x_{ckp} + \left(a_{2k} x_{ckw} - c_{\mathcal{W}_{s,t}} \right) + a_{0k} w_{ckp,t} \end{aligned} \tag{25}$$

In Eq. (25), the variable w denotes the state of power x_{pi}, water x_{wj} and cogeneration $x_{ckp,ckw}$ facilities. In the cogeneration power and water networks, the additional water storage constraint $c_{\mathcal{W}_{s,t}}$ is included. The objective function (Eq. (24)) has associated constraints in power, water, and cogeneration networks, respectively. Where the power flow balance Eq. (26) is modified to specifically include the cogeneration and storage facilities:

$$P_{D_i} - \left\{ \sum_{k=1}^{n_{cp}} I_{cky} x_{ckp} - \sum_{i=1}^{n_{pp}} I_{piy} x_{pi} + \sum_{y=1}^{m_p} B_{yz}(\delta_y - \delta_z) \right\} 0 = \qquad \forall y = 1, \ldots, m_p. \tag{26}$$

where, I_{cky} and I_{piy} denote incidence matrices for water and power networks and m_p denotes the number of lines in power distribution network.

$$0 = D_{wa} - \left(\sum_{k=1}^{n_{cp}} I_{ckt} x_{cwk} - \sum_{j=1}^{n_{wp}} I_{wjt} x_{wj} + \sum_{a=1}^{m_w} F_{ab} + \sum_{s=1}^{n_{sp}} \mathcal{W}_s \right) \qquad \forall y = 1, \ldots, m_w. \tag{27}$$

Similarly, the cogeneration plants add the water balance equation (Eq. (27)), which denotes the water supply and demand balance expression including the coproduction and water storage system. In contrast, m_w denotes the number of lines in the water distribution network.

$$D_{wa} = \left\{ D^{pi}_{wa,t} + D^{wj}_{wa,t} + D^{ckp}_{wa,t} + D^{ckw}_{wa,t} + D^{\mathcal{W}_s}_{wa,t} \right\}, \quad \forall t \in T, i \in m_p, j \in m_w, k \in m_{cp}. \tag{28}$$

where, Eq. (28) denotes the total water demand at power, water, cogeneration and storage plants, respectively.

$$w_{pi,t} = \left(u_{pi,t} - v_{pi,t} + w_{pi,t-1} \right) + \left(u_{ps,t} - v_{ps,t} + w_{ps,t-1} \right), \forall i \in n_{pp}, t \in T. \tag{29}$$

Here, u denotes the state-up, v denotes the shut-down, and w denotes the ON/OFF states of all generation facilities, respectively. In Eq. (29), the expression $\left(u_{pi,t} - v_{pi,t} + w_{pi,t-1} \right)$ denotes the switching states of the power generation plant, while the expression $\left(u_{ps,t} - v_{ps,t} + w_{ps,t-1} \right)$ denotes the switching states of water storage facilities. However, this work does not include the power storage faculties.

$$\begin{aligned} w_{wj,t} = & \left(u_{wj,t} - v_{wj,t} + w_{wj,t-1} \right) + \left(u_{\mathcal{W}_{s,wj,t}} - v_{\mathcal{W}_{s,wj,t}} + w_{\mathcal{W}_{s,wj,t-1}} \right), \\ & \forall j \in n_{wp}, s \in n_{sp}, t \in T. \end{aligned} \tag{30}$$

In Eq. (30), the expression $\left(u_{wj,t} - v_{wj,t} + w_{wj,t-1} \right)$ denotes the switching states of water generation plant, while the expression $\left(u_{\mathcal{W}_{s,wj,t}} - v_{\mathcal{W}_{s,wj,t}} + w_{\mathcal{W}_{s,wj,t-1}} \right)$ denotes the switching states of water storage facility.

$$\begin{aligned} & w_{ck,t} = \left(u_{ckp,t} - v_{ckp,t} + w_{ckp,t-1} \right) + \left(u_{\mathcal{W}_{s,ckp,t}} - v_{\mathcal{W}_{s,ckp,t}} + w_{\mathcal{W}_{s,ckp,t-1}} \right) +, \ldots \\ & \left(u_{ckw,t} - v_{ckw,t} + w_{ckw,t-1} \right) + \left(u_{\mathcal{W}_{s,ckw,t}} - v_{\mathcal{W}_{s,ckw,t}} + w_{\mathcal{W}_{s,ckw,t-1}} \right), \\ & \forall k \in n_{ck}, s \in n_{sp}, t \in T. \end{aligned} \tag{31}$$

Finally, the Eq. (31) denotes the switching states of generation and storage facilities in cogeneration power and water networks, respectively.

$$u_{pi,t} + v_{pi,t} = 1, \forall i \in n_{pp}, t \in T. \tag{32}$$

$$u_{wj,t} + v_{wj,t} = 1, \forall j \in n_{wp}, t \in T. \tag{33}$$

$$u_{ckp,j,t} + v_{ckp,j,t} = 1, \forall j \in n_{ckp}, t \in T. \tag{34}$$

$$u_{ckw,j,t} + v_{ckw,j,t} = 1, \forall j \in m_{ckw}, t \in T. \tag{35}$$

$$u_{\mathcal{W}_{s,t}} + v_{\mathcal{W}_{s,t}} = 1, \forall s \in n_{sp}, \forall t \in T. \tag{36}$$

Where, Eqs. (32), (33), (34), (35) and (36) ensure that dispatchable generation facilities, combined power plants (32), water plants (33), cogeneration plants ((34), (35)) and storage resources (36) that are simultaneously dispatched are not allowed to start-up $u_{pi} = 1$ and/or shut-down $v_{pi} = 1$, at the same time to ensure supply–demand balance.

4.1. Power & Water generation limits

The optimization objective aims to reduce total operational costs while adhering to generation capacity limits for power, water, cogeneration, and storage systems. These constraints ensure the system operates within its capacity, enhancing stability and efficiency across the network. The generation and storage limits are formally defined as:

$$\begin{aligned} \underline{GenPP} \le X_p \le \overline{GenPP}, \\ \underline{GenWP} \le X_w \le \overline{GenWP}, \\ \underline{GenCPP} \le X_{cpp} \le \overline{GenCPP}, \\ \underline{GenCPW} \le X_{cpw} \le \overline{GenCPW}, \\ \underline{Gen\mathcal{W}_s} \le X_s \le \overline{Gen\mathcal{W}_s}. \end{aligned} \tag{37}$$

Eq. (37) establishes the permissible operational bounds for power generation (X_p), water production (X_w), cogeneration of power (X_{cpp}),

cogeneration of water (X_{cpw}), and water storage capacity (X_s). These constraints are critical for maintaining a balanced and stable production environment, minimizing the risk of operational failures and ensuring a reliable supply of power and water.

4.2. Flow limits

Flow limits for power and water within the network are essential for operational stability and efficiency, as outlined below:

$$\begin{aligned} \underline{PFlow_{ij}} &\le B_{ij}(\delta_i - \delta_j) \le \overline{PFlow_{ij}} \\ \underline{WFlow_{tu}} &\le Q_{tu} \le \overline{WFlow_{tu}}. \end{aligned} \tag{38}$$

These constraints, crucial for minimizing transmission losses as discussed in Section 4.1, regulate the flow between nodes to ensure it remains within safe and efficient operational bounds; thereby supporting the system's overall production capacity and adherence to environmental standards.

4.3. Storage limit & Continuity relation

Beyond flow limits, water storage facilities are subject to capacity constraints to ensure supply continuity and demand fulfillment:

$$\underline{Store\mathcal{W}_s} \le \mathcal{W}_s(t) \le \overline{Store\mathcal{W}_s} \quad \forall t,\ \forall v = 1...n_v. \tag{39}$$

Moreover, the continuity of water storage operations is maintained as follows:

$$\mathcal{W}_s(t) = \mathcal{W}_s(t-1) - X_{\mathcal{W}_s}(t) \quad \forall t,\ \forall v = 1...n_v. \tag{40}$$

4.4. Initial conditions

The initial condition of water storage facility is taken as a constraint in Eq. (41).

$$\mathcal{W}_s(t) = 0 \quad \forall t,\ \forall v = 1...n_v. \tag{41}$$

These limits (Eqs. (39), (40), (41)) are flexible and may be adjusted over time according to water generation and demand variations. These are also helpful for short, medium, or long-term water management goals.

4.5. Coproduction process limits

Coproduction process limits in terms of combined power and water generation facilities are given as:

$$\underline{r_k} \le \frac{x_{ckp}}{x_{ckw}} \le \overline{r_k} \tag{42}$$

Eq. (42) is not used to control the power and water flows to the cogeneration plants. Instead, this expression is used for the safe operation of cogeneration facilities and allows the plants to automatically adjust their limits based on the requirements.

4.6. Ramping limits

Ramping limits of the three types of generation facilities are given as;

$$\left[\underline{RRP_i}\right] \le x_{pi}(t) - x_{pi}(t-1) \le \left[\overline{RRP_i}\right], \forall i = 1...n_{pp} \tag{43}$$

$$\left[\underline{RRW_j}\right] \le x_{wj}(t) - x_{wj}(t-1) \le \left[\overline{RRW_j}\right], \forall j = 1...n_{wp} \tag{44}$$

$$\left[\frac{\underline{RRCP_k}}{\underline{RRCP_k}}\right] \le x_{ckp}(t) - x_{ckp}(t-1) \le \left[\frac{\overline{RRCP_k}}{\overline{RRCP_k}}\right], \forall i = 1...n_{ckp} \tag{45}$$

$$\left[\frac{\underline{RRCW_k}}{\underline{RRCW_k}}\right] \le x_{ckw}(t) - x_{ckw}(t-1) \le \left[\frac{\overline{RRCW_k}}{\overline{RRCW_k}}\right], \forall i = 1...n_{ckw} \tag{46}$$

$$\left[\underline{RR\mathcal{W}_s}\right] \le x_{\mathcal{W}_s}(t) - x_{\mathcal{W}_s}(t-1) \le \left[\overline{RR\mathcal{W}_s}\right], \forall i = 1...n_s \tag{47}$$

Eqs. ((43), (44), (45), and (47)) denote ramping limits to give preferences to the generation plants to meet the power and water demand requirements.

5. Simulation setup

The system model (outlined in Section 3) is applied to test cases involving power, water and food processing units based on the datasets (Tables 3, 4, 5, 6, 7). These datasets were selected for their variability in power and water demand, accurately reflecting real-world usage patterns, and for demonstrating the demand ratio of power to water over time t. Fig. 4 presents the demand profiles for power and water over t. To manage peak demands, the model includes two water storage facilities at nodes 2&6. For implementation, the integration of the General Algebraic Modeling System (GAMS) and MATLAB tools is employed. GAMS facilitates optimization using the CONOPT solver, renowned for its capability to manage large-scale optimization problems, whereas MATLAB is utilized for efficient data management and visualization purposes. The results section is further divided into two sections. The Section 5.1 discusses about the power and water generation profiles along with the cogeneration relationships. The Section 5.2 provides the details about the cost, storage, LMP and nodal cost of the power generation network, respectively.

5.1. Results

In Fig. 5, the power generation profiles over 24 h are shown, while Fig. 6 gives the water generation profiles under various ramping limit configurations over time t. These visualizations highlight that the ratio of power and water generation is not only impacted by demand ratios and specified upper and lower bounds but also by ramping limit settings towards minimizing total costs and meeting optimality criteria. Improper ramping configurations may result in higher costs due to non-optimal utilization of generation and production capacities. This is particularly notable as the demand profiles and variations analyzed in this study tend to yield more sophisticated optimization outcomes compared to commonly used demand profiles. Within the proposed model, coproduction facilities are always used as primary sources for meeting power and water demand, while individual power and water plants are typically included to address peak demand scenarios.

In Fig. 6, the water capacity utilized by both water and cogeneration networks is shown, highlighting the adaptation of generation profiles based on specified upper and lower bounds and ramping limits. For instance, as shown in Fig. 6(b), setting the water production limit to zero leads to an increased reliance on cogeneration facilities for water generation. Fig. 6(a, b) demonstrates an increased output from the water production facility, with cogeneration facilities serving as the primary option during operations. In cases where these conditions are not met, the optimization algorithm rearranges production schedules based on cost functions and process constraints. Further details regarding the calculation for power demand requirements are provided in Section 3.5. In addition, Fig. 6 highlights water storage levels, represented by black and red dotted lines in the web-based version, indicating a moderate quantity of water storage capacity.

In Fig. 7, the rationale behind prioritizing coproduction units as the "first choice" in response to fluctuating water and power demands over time (t) is highlighted. This strategy enables cogeneration facilities to operate at full capacity while maintaining product ratios, thereby minimizing overall costs. The profiles also illustrate power and water demand set points varying from 2 to 9 MW/m^3 in alignment with the demand ratio, while cogeneration facilities exhibit set points ranging from 2 to 12 MW/m^3. These values may adjust based on demand dynamics and ramping modifications, with water and power plants

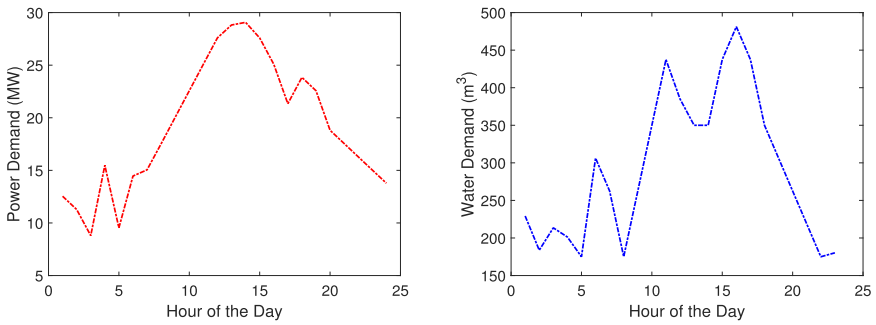

(a) Power demand profile. (b) Water demand profile.

Fig. 4. Power and water demand requirements over 24 h time.

Table 3
Plant and cost data (Rasheed and R-Moreno, 2021).

Plants	Indices	Max power (MW)	Max water (m^3/h)	Min Power (MW)	Min water (m^3/h)
Power	i_1	6.8	0	1.5	0
Power	i_2	3.0	0	0.5	0
Power	i_3	6.5	0	0.5	0
Power	i_4	6.5	0	1.5	0
Coproduction	k_1	6.5	140	0	0
Coproduction	k_2	2.8	100	1.5	0
Coproduction	k_3	2.8	140	0	0
Water	j_1	0	180	0	0

Table 4
Coproduction plant cost coefficients (Rasheed and R-Moreno, 2021).

Cost coefficient terms	A_{11}	A_{12}	A_{22}	A_1	A_2	A_0
Coproduction unit 1	44,330	3546	7093	1.106	4.426	737.4
Coproduction unit 2	78,810	6305	126.1	1.475	5.901	737.4
Coproduction unit 3	1773	141.9	283.7	2.213	8.851	737.4

Table 5
Power plant cost coefficients (Rasheed and R-Moreno, 2021).

Cost coefficient terms	A_1	A_2	A_0
P_{g_1}	57,140	9999.5	0
P_{g_2}	57,140	22,856.56	0
P_{g_3}	85,710	1428.5	0
P_{g_4}	85,710	1428.5	0

Table 6
Water plant cost coefficients (Rasheed and R-Moreno, 2021).

Cost coefficient terms	A_1	A_2	A_0
Water generation unit	18,341.94	0	104.2805

Table 7
Water demand in food processing industry (Ellis et al., 2009).

Sr. No.	Product	Min. water usage (m^3/t)	Max. water usage (m^3/t)
1	Beer	9.08	14.53
2	Milk products	9.08	18.16
3	Meat packing	13.62	18.16
4	Bread	1.81	3.64
5	Whisky	54.50	72.67
6	Green beans	45.42	64.35
7	Peaches and pears	13.62	18.16
8	Fruits and vegetables	3.64	31.79

serving as “second choice” during peak demand periods to optimize cost efficiency. However, without careful adjustment of ramping limits, there could be a risk of incurring higher costs due to inefficient

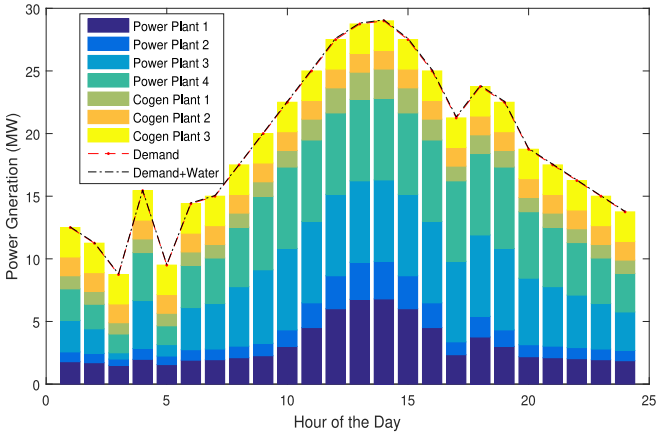

Fig. 5. Power generated by the single product power, water & cogeneration plants and the demand profile over 24 h period.

operation, either from overreliance on a single product or no-optimal use of a single cogeneration facility.

Fig. 8 shows the energy obtained from power facilities over 24 h, demonstrating the operation within upper and lower limits while meeting demand through coordinated co-dispatch. Notably, the power plants located at nodes 6 and 13 experience significant utilization, particularly during high-peak demand periods later in the day. In contrast, the plants located at nodes 2 and 3 observe moderate use, with demand partially met by by-product generation facilities. Similarly, Fig. 9 highlights water production profiles from single-product water facilities and storage units, which are co-dispatched to satisfy water demand for potable use and power generation. These profiles established bounds and constraints, ensuring that generation capacities and demand requirements are met without exceeding limits.

Fig. 10 shows the water production profile from cogeneration plants, which are co-dispatched to fulfill demand capacity requirements. Typically, these plants operate at maximum capacity to serve

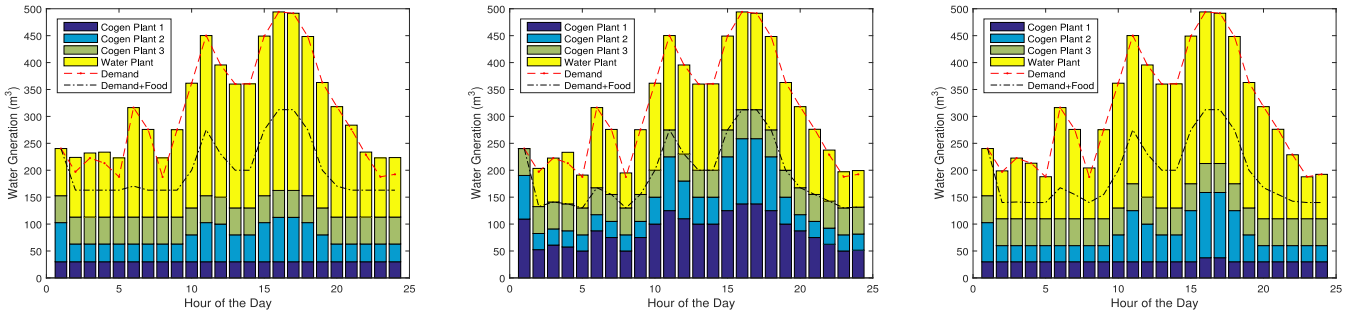

(a) Ramping limits (m^3) on cogeneration water plants: The minimum lower limits are (30, 30, 50), the maximum upper limits (200, 150, 120), and ramping limit of single product water plant: minimum lower limit (50), maximum upper limit (150)

(b) Ramping limits (m^3) on cogeneration water plants: The minimum lower limts are (30, 30, 50), the maximum upper limits are (200, 150, 120), and ramping limit on single product water plant: minimum lower limit is (0), maximum upper limit is (0)

(c) Ramping limits (m^3) on cogeneration water plants: The minimum lower limits are (30, 30, 50), the maximum upper limits are (200, 150, 120), and ramping limit on single product water plant: minimum lower limit is (30), maximum upper limit is (100)

Fig. 6. Water generation and demand profiles against different settings of ramping limits over 24 h period.

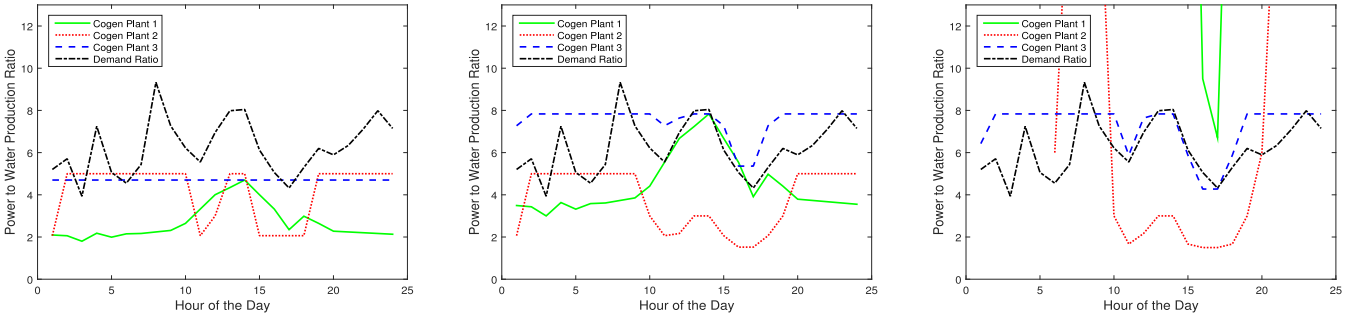

(a) Limits (m^3) on cogen. water plants: min. (50, 30, 50), max. (140, 200, 100)

(b) Limits (m^3) on cogen. water plants: min. (30, 30, 30), max. (100, 100, 100)

(c) Limits (m^3) on cogen. water plants: min. (0, 0, 30), max. (140, 200, 100)

Fig. 7. The demand relation between the power and water for the coproduction over 24 h period.

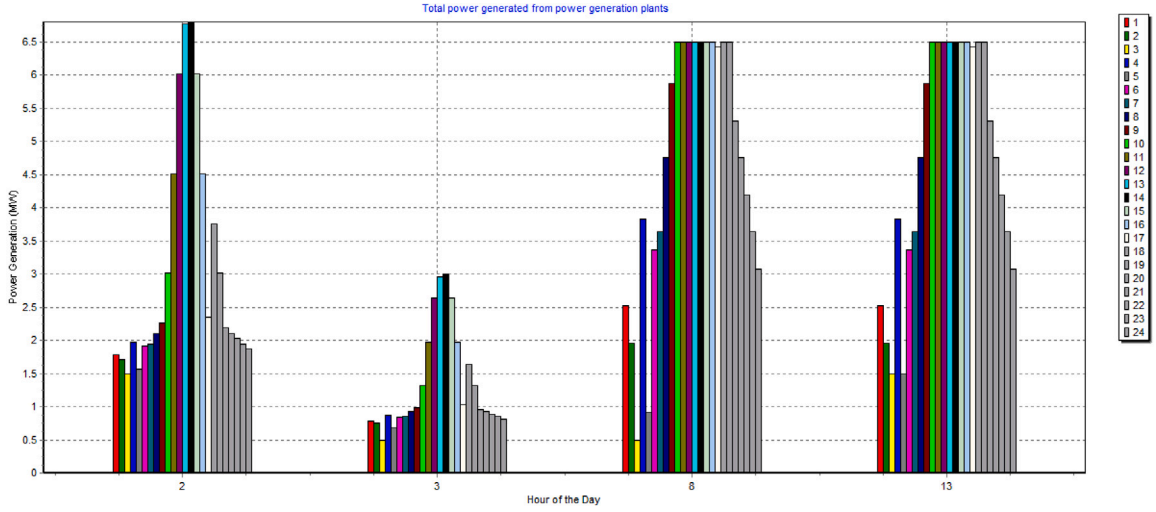

Fig. 8. Total power generated from different power generation units located at nodes 2, 3, 8 and 13 (Fig. 2) over the period of 24 h., (at y-axis).

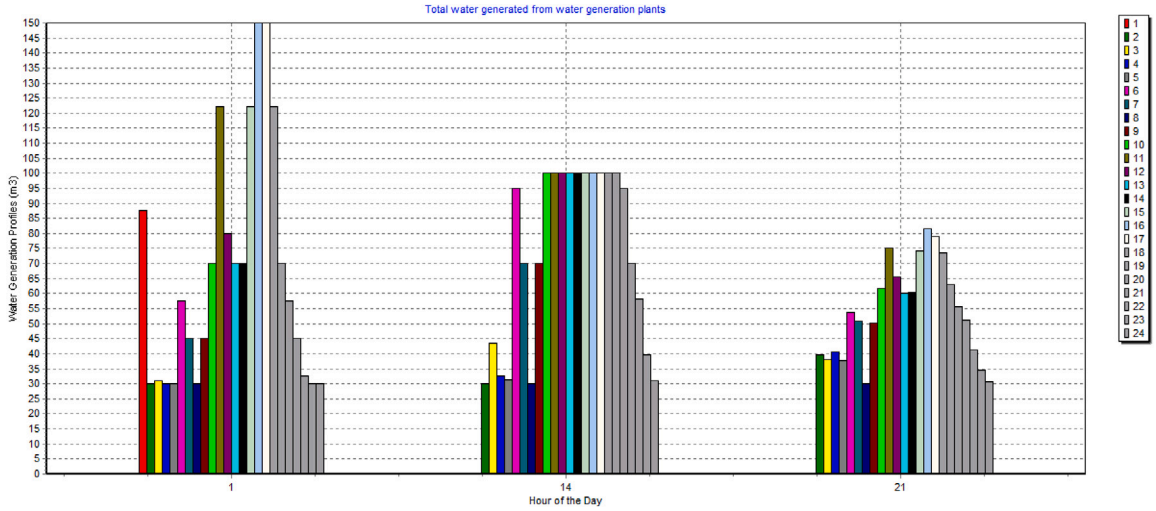

Fig. 9. Water generated from single product water and storage units attached at nodes 1, 14 and 21 over the period of 24 h. The capacity at negative hours represents the surplus water that is stored in the water storage facilities to alleviate the pressure on cogeneration facilities during peak demand hours.

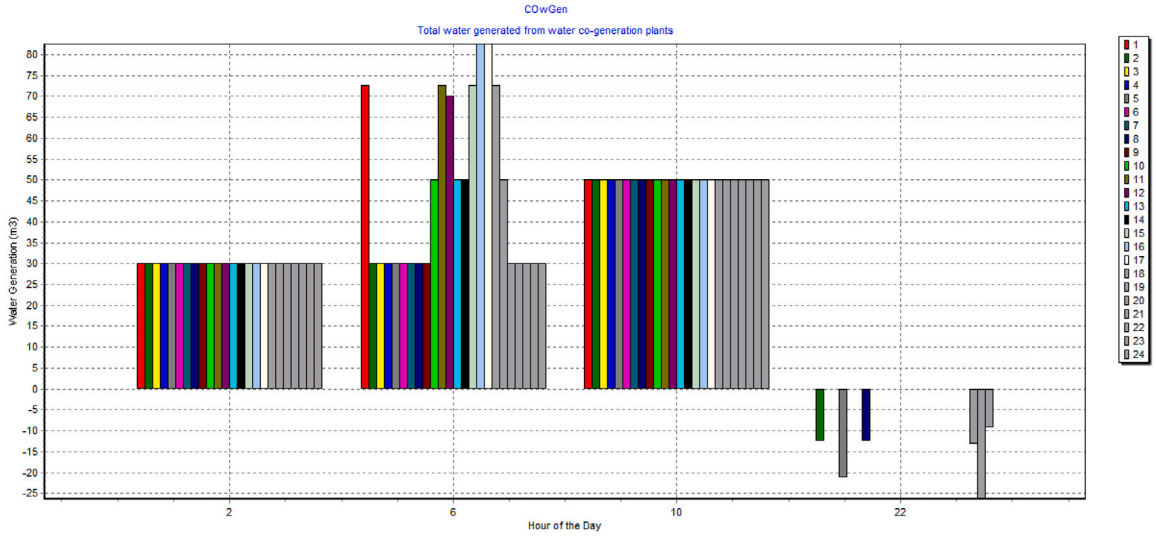

Fig. 10. Water production profiles of different water coproduction units over 24 h.

as the primary source for meeting demand. Additionally, any surplus capacity is conserved in integrated storage tanks. This strategy alleviates demand pressure during peak hours, reducing the need to depend on more expensive generation resources, and thereby lowering overall costs.

The power and water demand profiles are based on observations from real-time test cases, reflecting typical consumption patterns. For instance, industrial activities, which intensify in the afternoon, lead to significant peaks in power demand. As depicted in Fig. 4, these peaks predominantly occur from hour 10 (h_{10}) to hour 16 (h_{16}), whereas the lowest power demand is observed in the early hours, specifically from hour 1 (h_1) to hour 3 (h_3).

Similarly, water demand exhibits distinctive peaks at several points during the day: an initial surge around hour 6 (h_6), with further increases from hour 10 (h_{10}) to hour 16 (h_{16}) and extending to hour 18 (h_{18}). The early morning peak corresponds to water usage for irrigation, highlighting the agricultural sector's impact. The later spikes are attributable to increased consumption within industrial and commercial sectors.

5.2. Section-II: Storage & Power generation costs

Fig. 11 presents an analysis of hourly costs associated with power, water, and cogeneration plants, showcasing the cost dynamics under different operational strategies and constraints. The illustration underscores the variability in costs, particularly emphasizing the heightened expenses encountered during peak demand periods. Additionally, it highlights the relatively higher cost burden shouldered by coproduction plants, despite a generally uniform cost structure across various types of facilities. Fig. 11(a) illustrates the optimal cost scenario obtained through efficient utilization of generation and production facilities. Similarly, Fig. 11(b) demonstrates higher costs due to ramping constraints on cogeneration facilities, highlighting the financial impact of operational limitations. To address demand requirements, the optimization program prioritized single-product water production facilities, ensuring full utilization of cogeneration facilities within imposed constraints. Fig. 11(c) demonstrates a cost reduction achieved by setting lower ramping limits to zero and increasing upper ramping limits, resulting in water obtained primarily from single-product facilities with minimal intake from by-product facilities. While this strategy

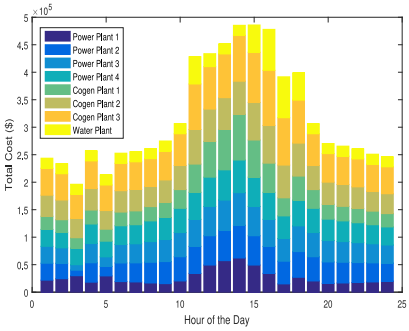

(a) Limits (MW) on cogeneration power plants: The minimum lower limits are (50,30,50), the maximum upper limits are (140,200,100)

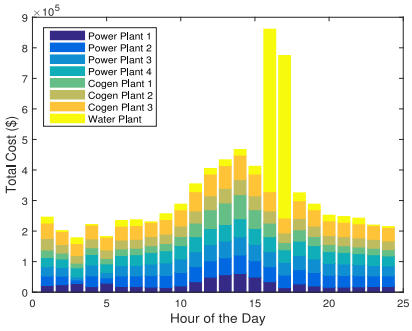

(b) Limits (MW) on cogeneration power plants: The minimum lower limits are (30,30,30), the maximum upper limits are (100,100,100)

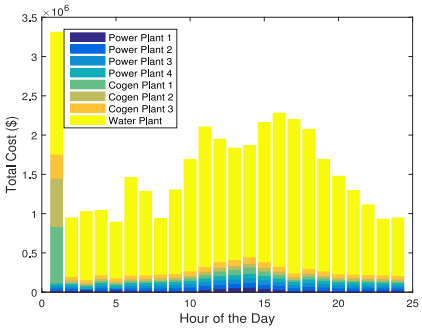

(c) Limits (MW) on cogen. water plants: min. (0,0,30), max. (140,200,100)

Fig. 11. Cost incurred by different power and cogeneration plants for 24 h.

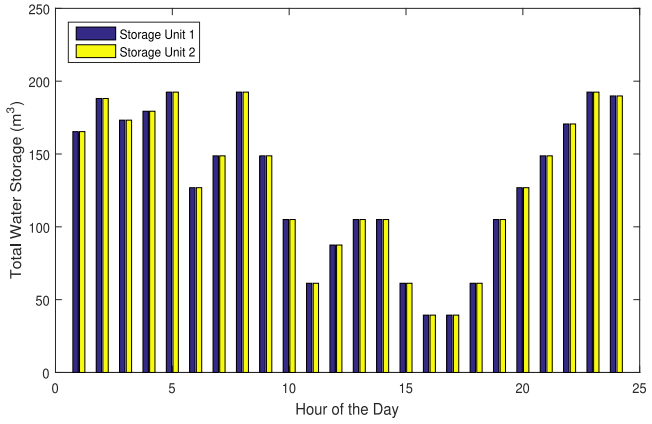

Fig. 12. The amount of water capacity stored in units 1 &2 profile over 24 h.

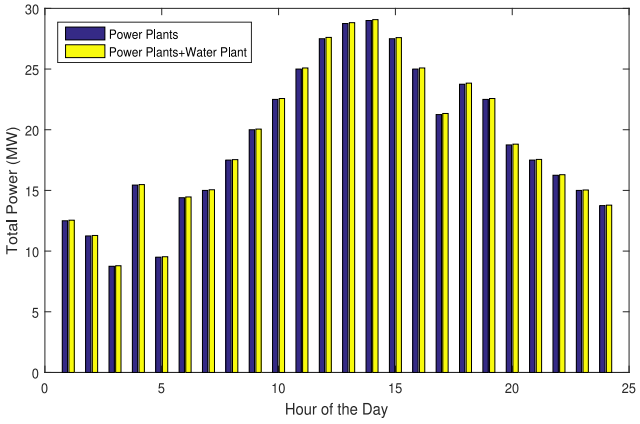

Fig. 13. A comparison of power consumed by power and water pumping networks.

decreased total costs, it led to suboptimal utilization across all plants. The water storage profile over 24 h is shown in Fig. 12. According to the mathematical model, the storage begins from zero as an initial condition and grows during the periods (i.e., h_{11} to h_{19}) of low demand. From h_1 to h_{10}, the quantity of stored water is high due to low demand and vice versa. The stored water could be used when water demand is higher, since, the water usage from storage plants is dependent on two factors: (i) the diameter of the pipe, and (ii) the water flow rate. However, the capacity of water storage plants is quite high. Fig. 13 shows the comparison of energy usage in power and water networks, respectively.

In the water network, energy from the power network (specifically, node 28 as shown in Fig. 2) powers a water pump. This pump operates on minimal energy during peak demand hours, leading to lower power consumption in comparison to the continuous operation of power plants. Fig. 14 illustrates the LMPs at different buses (nodes) affected by congestion on transmission lines. Without incorporating limits on transmission lines, power networks exhibit uniform prices across nodes. Contrarily, under DCOPF conditions, where line resistance is assumed to be negligible, LMPs are determined based on congestion costs through the use of shift factors, highlighting the impact of transmission limitations on pricing dynamics.

Fig. 15 shows power generation costs at each bus within a modified IEEE standard bus system topology, reflecting dynamic trends in load demand and the contribution of co-generation capacity from dual-product plants. These plants are co-dispatched, impacted by both nodal

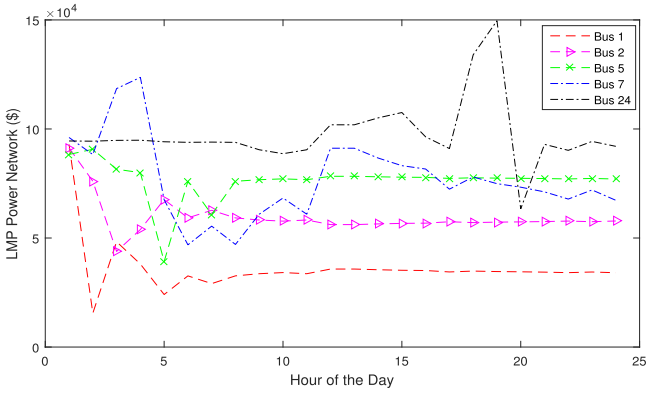

Fig. 14. LMP of the modified IEEE 30 bus network. The LMPs shown here are taken randomly to visualize the nodal cost when the demand requirement changes.

and overall pricing in the power network. Additionally, Table 8 gives cost and CO_2 emission profiles for power, water, and cogeneration plants, operated according to various water supply scenarios. Variability in cogeneration plant costs arises from changes in water supply across network nodes (nodes 1-5), requiring reliance on single-product power and water plants, which are generally more expensive, with costs ranging between $1.96E03$–$3.10E05$. Table 8 further highlights operational settings of water and cogeneration plants, emphasizing the

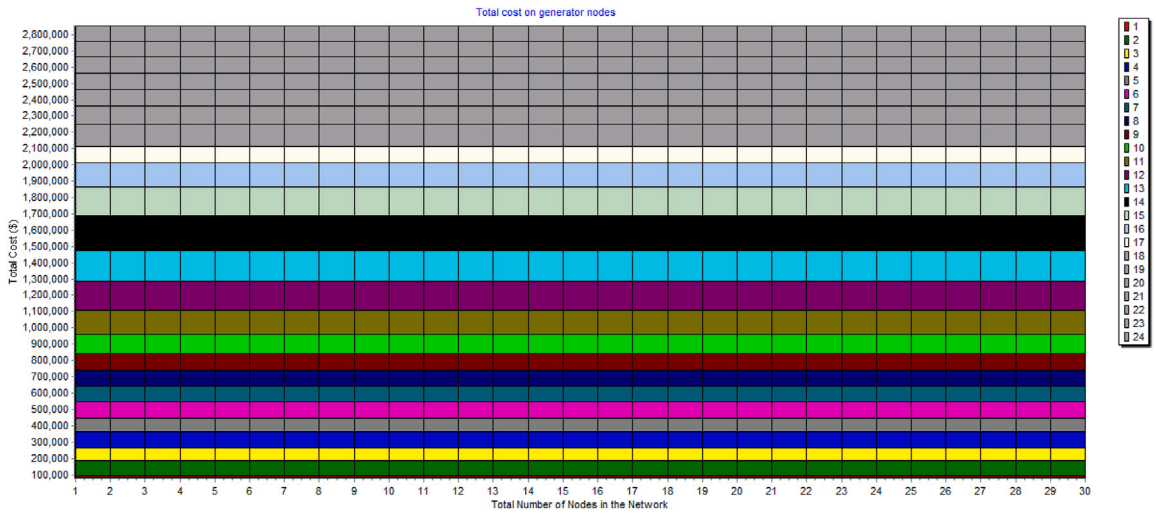

Fig. 15. Individualized nodal (at x-axis) cost profile of different power generation units over the period of 24 h., (at y-axis).

Table 8
A comparison of the cost ($) and CO_2 emissions at various settings.

Setting	Power plants				Cogeneration plants						Water plant	Total cost	% increase	CO_2/kg	% increase
	P1	P2	P3	P3	Cogen. 1		Cogen. 2		Cogen. 3		W1				
					Power	Water	Power	Water	Power	Water					
1	6.52E+5	2.82E+5	9.43E+5	9.74E+5	7.70E+5	3.60E+3	8.11E+5	8.73E+3	1.27E+6	6.01E+3	3.35E+5	3,209,000		7,669,510	
2	6.52E+5	2.82E+5	9.43E+5	9.74E+5	7.70E+5	7.05E+5	8.11E+5	5.23E+5	1.27E+6	3.23E+5	2.99E+7	34,300,000	3.10E+5	81,977,000	968.869
3	6.52E+5	2.82E+5	9.43E+5	9.74E+5	7.70E+5	0.00E+0	8.11E+5	1.09E+4	1.27E+6	7.47E+3	2.99E+7	32,772,000	2.95E+5	78,325,080	921.253
4	6.52E+5	2.82E+5	9.43E+5	9.74E+5	7.70E+5	0.00E+0	8.11E+5	2.28E+4	1.27E+6	0.00E+0	5.31E+5	34,05,000	1.96E+3	8,137,950	6.10782
5	6.52E+5	2.82E+5	9.43E+5	9.74E+5	7.70E+5	1.14E+4	8.11E+5	0.00E+0	1.27E+6	2.29E+4	1.63E+6	4,513,000	1.30E+4	10,786,070	40.6357

efficiency of the proposed model (Setting-1, Fig. 11a), which achieves lower costs and CO_2 emissions.

Setting 2 demonstrates that if the water supply at cogeneration plant-3 is reduced, the demand capacity is met through cogeneration plant-1. However, increased capacity production at cogeneration plant-3 increased its cost, resulting in higher total cost and carbon emissions. Setting 3 reveals that reducing the water supply at cogeneration plant-1 to zero boosts water utilization at cogeneration plant-3, leading to elevated costs and carbon emissions. Similarly, settings 4 and 5 depict increased costs of cogeneration plants due to decreased water supply to cogeneration plants 1–3. Additionally, heavy reliance on single-product power and water plants incurs increased costs and CO_2 emissions ranging from 6%–969% based on the power and water demand ratio. The table underscores that the proposed algorithm operates at optimal set points to minimize potential costs and CO_2 emissions.

6. Conclusions

In this study, an advanced Energy–Water–Food Nexus (EWFN) model is developed for the co-dispatch of power, water, and storage capacities, integrating flow limits into the optimization framework. Building upon previous research, this model introduces enhancements such as water storage units, ramping constraints, and continuity relationships, which were notably absent in earlier studies. These additions effectively address the limitations of former models, particularly in terms of flow limits, storage facilities, water junction models, and LMPs. The proposed model has minimized total costs across power, water, and cogeneration plants, incorporating a comprehensive set of constraints related to generation, demand, processing, storage, transmission, and continuity. Our evaluation, utilizing a dataset spanning power, water, and food networks, focused on a hypothetical system comprising four power plants, one pure water plant, three cogeneration plants, and a storage facility. Our findings underscore a significant role for cogeneration and combined power and water plants in managing initial demand, overshadowing single-product plants due to their higher operational costs. A notable impact is observed on water storage facilities in reducing total costs, highlighting dual utility in both power and water networks. The joint optimization algorithm successfully optimized generation resources by selecting optimal set points within the defined constraints. However, it also raised critical concerns regarding the challenges of integration within the co-optimization framework.

The integration and optimization strategies developed in this study have significant implications for advancing cleaner production technologies. By enabling more efficient use of resources and reducing operational costs and carbon emissions, the model promotes the broader adoption of cleaner technologies in various sectors. The dual utility of water storage facilities not only optimizes resource management but also encourages the adoption of integrated solutions that are environmentally sustainable and economically viable. Additionally, the successful application of cogeneration highlights the potential for these technologies to replace more resource-intensive systems, further fostering a shift towards cleaner production methods.

Future advancements of the proposed model will focus on enhancing cross-sector synergies and resilience under climate change. The main goal will be to explore sustainable circular economy strategies, where integration and interdependencies among sectors are leveraged for mutual benefit, such as using agricultural waste in bioenergy production or recycling water resources. Simultaneously, the model will be adapted to assess and mitigate the impacts of climate change, integrating climate projections to understand potential disruptions and developing adaptive and dynamic strategies for extreme weather events and long-term climatic shifts. By doing so, the model will not only provide a comprehensive framework for sustainable resource management but also ensure resilience in the face of evolving environmental challenges, thus contributing to global sustainability efforts.

CRediT authorship contribution statement

Muhammad Babar Rasheed: Writing – review & editing, Writing – original draft, Visualization, Validation, Software, Methodology, Formal analysis, Data curation, Conceptualization. **María D. R-Moreno:** Writing – review & editing, Writing – original draft, Investigation, Funding acquisition, Formal analysis, Conceptualization.

Declaration of competing interest

The authors declare that they have no known competing financial interests or personal relationships that could have appeared to influence the work reported in this paper.

Data availability

No data was used for the research described in the article.

Acknowledgments

This project has received funding from the European Union Horizon 2020 research and innovation programme under the Marie Sklodowska-Curie grant agreement No 754382, GOT ENERGY TALENT.

References

Al-Adwani, A., Karnib, A., Elsadek, A., Al-Zubari, W., 2023. Scenario-based assessment of the water-energy-food nexus in Kuwait: Insights for effective resource management. Comput. Water Energy Environ. Eng. 13, 38–57.

Al-Ansari, T., Korre, A., Nie, Z., Shah, N., 2017. Integration of greenhouse gas control technologies within the energy, water and food nexus to enhance the environmental performance of food production systems. J. Clean. Prod. 162, 1592–1606.

Averyt, K., Macknick, J., Rogers, J., Madden, N., Fisher, J., Meldrum, J., Newmark, R., 2013. Water use for electricity in the united states: An analysis of reported and calculated water use information for 2008. Environ. Res. Lett. 8, 015001.

Ban, M., Yu, J., Shahidehpour, M., Yao, Y., 2017. Integration of power-to-hydrogen in day-ahead security-constrained unit commitment with high wind penetration. J. Mod. Power Syst. Clean Energy 5, 337–349.

Coulbeck, B., 1980. Dynamic simulation of water distribution systems. Math. Comput. Simulation 22, 222–230.

Ellis, M., Dillich, S., Margolis, N., 2009. Industrial Water Use and Its Energy Implications, Prepared By Energetics Incorporated for the Us Department of Energy. Office of Energy Efficiency and Renewable Energy, Office of Industrial Technologies, Washington, DC.

Farid, A.M., Lubega, W.N., 2013. Powering & watering agriculture: Application of energy-water nexus planning. In: 2013 IEEE Global Humanitarian Technology Conference. GHTC, IEEE, pp. 248–253.

Ghobadian, R., Mohammadi, K., 2023. Optimal design and cost analysis of water distribution networks based on pressure-dependent leakage using nsga-ii. Appl. Water Sci. 13, 92.

Haggi, H., Sun, W., Fenton, J.M., Brooker, P., 2021. Risk-averse cooperative operation of pv and hydrogen systems in active distribution networks. IEEE Syst. J. 16, 3972–3981.

Haktanır, T., Ardıçlıoğlu, M., 2004. Numerical modeling of Darcy–Weisbach friction factor and branching pipes problem. Adv. Eng. Softw. 35, 773–779.

He, G., Mallapragada, D.S., Bose, A., Heuberger, C.F., Gençer, E., 2021. Hydrogen supply chain planning with flexible transmission and storage scheduling. IEEE Trans. Sustain. Energy 12, 1730–1740.

Kanyerere, T., Tramberend, S., Levine, A.D., Mokoena, P., Mensah, P., Chingombe, W., Goldin, J., Fatima, S., Prakash, M., 2018. Water futures and solutions: Options to enhance water security in Sub-Saharan Africa. Syst. Anal. Approach Complex Glob. Chall. 93–111.

Leeton, U., Uthitsunthorn, D., Kwannetr, U., Sinsuphun, N., Kulworawanichpong, T., 2010. Power loss minimization using optimal power flow based on particle swarm optimization. In: ECTI-CON2010: The 2010 ECTI International Confernce on Electrical Engineering/Electronics, Computer, Telecommunications and Information Technology. IEEE, pp. 440–444.

Li, Q., Yu, S., Al-Sumaiti, A.S., Turitsyn, K., 2018. Micro water–energy nexus: Optimal demand-side management and quasi-convex hull relaxation. IEEE Trans. Control Netw. Syst. 6, 1313–1322.

Lin, W., Yang, Z., Yu, J., Li, W., 2021. Transmission expansion planning with feasible region of hydrogen production from water electrolysis. IEEE Trans. Ind. Appl. 58, 2863–2874.

Lubega, W.N., Farid, A.M., 2014. An engineering systems model for the quantitative analysis of the energy-water nexus. In: Complex Systems Design & Management: Proceedings of the Fourth International Conference on Complex Systems Design & Management CSD & M 2013. Springer, pp. 219–231.

Mueller, T., 2023. When policy entrepreneurs drift between levels: The creation of the international renewable energy agency. Global Policy 14, 588–599.

Ngammuangtueng, P., Nilsalab, P., Chomwong, Y., Wongruang, P., Jakrawatana, N., Sandhu, S., Gheewala, S.H., 2023. Water-energy-food nexus of local bioeconomy hub and future climate change impact implication. J. Clean. Prod. 399, 136543.

Norouzi, N., 2022. Presenting a conceptual model of water-energy-food nexus in iran. Curr. Res. Environ. Sustain. 4, 100119.

Pan, G., Gu, W., Lu, Y., Qiu, H., Lu, S., Yao, S., 2020. Optimal planning for electricity-hydrogen integrated energy system considering power to hydrogen and heat and seasonal storage. IEEE Trans. Sustain. Energy 11, 2662–2676.

Peña-Torres, D., Boix, M., Montastruc, L., 2024. Multi-objective optimization and demand variation analysis on a water energy food nexus system. Comput. Chem. Eng. 180, 108473.

Probst, E., Fader, M., Mauser, W., 2024. The water-energy-food-ecosystem nexus in the danube river basin: Exploring scenarios and implications of maize irrigation. Sci. Total Environ. 914, 169405.

Rasheed, M.B., R-Moreno, M.D., 2021. The energy-water-food nexus architecture for the optimal resource allocation. In: 2021 IEEE PES Innovative Smart Grid Technologies Europe. ISGT Europe, IEEE, pp. 1–5.

Rogers, J., 2013. Water-smart power: Strengthening the us electricity system in a warming world.

Salomons, E., 2010. Watering-Water Distribution System Design and Analysis. EPANET, pp. 1–10.

Santhosh, A., Farid, A.M., Youcef-Toumi, K., 2013. Optimal network flow for the supply side of the energy-water nexus. In: 2013 IEEE International Workshop on Intelligent Energy Systems. IWIES, IEEE, pp. 155–160.

Santhosh Apoorva, A.M.F., Youcef-Toumi, K., 2014. Real-time economic dispatch for the supply side of the energy-water nexus. Appl. Energy 122, 42–52.

Schoonenberg, W.C., Farid, A.M., 2022. Hetero-functional network minimum cost flow optimization: A hydrogen–natural gas network example. Sustain. Energy Grids Netw. 31, 100749.

Schröder, J., Jörling, K., Reshma Carmel Francy, F., von Zitzewitz, E., Zangerl, K., 2021. The role of hydrogen for the energy transition in the uae and germany a joint study by the emirati-german energy partnership.

Shahidehpour, M., Bartucci, C., Patel, N., Hulsebosch, T., Burgess, P., Buch, N., 2015. Streetlights are getting smarter: Integrating an intelligent communications and control system to the current infrastructure. IEEE Power Energy Mag. 13, 67–80.

Stott, B., Jardim, J., Alsaç, O., 2009. Dc power flow revisited. IEEE Trans. Power Syst. 24, 1290–1300.

Sun, W., Harrison, G.P., 2021. Active load management of hydrogen refuelling stations for increasing the grid integration of renewable generation. IEEE Access 9, 101681–101694.

Tao, Y., Qiu, J., Lai, S., Zhao, J., 2020. Integrated electricity and hydrogen energy sharing in coupled energy systems. IEEE Trans. Smart Grid 12, 1149–1162.

Teng, Y., Wang, Z., Li, Y., Ma, Q., Hui, Q., Li, S., 2019. Multi-energy storage system model based on electricity heat and hydrogen coordinated optimization for power grid flexibility. CSEE J. Power Energy Syst. 5, 266–274.

Trifkovic, M., Sheikhzadeh, M., Nigim, K., Daoutidis, P., 2013. Modeling and control of a renewable hybrid energy system with hydrogen storage. IEEE Trans. Control Syst. Technol. 22, 169–179.

Uen, T.S., Chang, F.J., Z.Y.T.W., 2018. Exploring synergistic benefits of water-food-energy nexus through multi-objective reservoir optimization schemes. Sci. Total Environ. 134, 88–93.

Wang, X., Huang, W., Wei, W., Tai, N., Li, R., Huang, Y., 2021. Day-ahead optimal economic dispatching of integrated port energy systems considering hydrogen. IEEE Trans. Ind. Appl. 58, 2619–2629.

Xiao, Y., Wang, X., Pinson, P., Wang, X., 2017. A local energy market for electricity and hydrogen. IEEE Trans. Power Syst. 33, 3898–3908.

Zaiter, I., Ramadan, M., Bouabid, A., El-Fadel, M., Mezher, T., 2023. Potential utilization of hydrogen in the uae's industrial sector. Energy 128108.

Zarei, M., 2020. The water-energy-food nexus: A holistic approach for resource security in Iran, Iraq, and Turkey. Water-Energy Nexus 3, 81–94.